TlP5: An unexplored direct band gap 2D semiconductor with ultra-high carrier mobility

Jun-Hui Yuan, Alessandro Cresti, Kan-Hao Xue, Ya-Qian Song, Hai-Lei Su, Li-Heng Li, Nai-Hua Miao, Zhi-Mei Sun, Jia-Fu Wang, Xiang-Shui Miao

▶ **To cite this version:**

Jun-Hui Yuan, Alessandro Cresti, Kan-Hao Xue, Ya-Qian Song, Hai-Lei Su, et al.. TlP5: An unexplored direct band gap 2D semiconductor with ultra-high carrier mobility. Journal of Materials Chemistry C, 2019, 7 (3), pp.639. 10.1039/C8TC05164J . hal-01964878

HAL Id: hal-01964878
https://hal.science/hal-01964878v1

Submitted on 19 Nov 2020

HAL is a multi-disciplinary open access archive for the deposit and dissemination of scientific research documents, whether they are published or not. The documents may come from teaching and research institutions in France or abroad, or from public or private research centers.

L'archive ouverte pluridisciplinaire **HAL**, est destinée au dépôt et à la diffusion de documents scientifiques de niveau recherche, publiés ou non, émanant des établissements d'enseignement et de recherche français ou étrangers, des laboratoires publics ou privés.

TlP_5: An unexplored direct band gap 2D semiconductor with ultra-high carrier mobility

Jun-Hui Yuan,[1] Alessandro Cresti,[2] Kan-Hao Xue,[1,2] Ya-Qian Song,[1] Hai-Lei Su,[1] Li-Heng Li,[1] Nai-Hua Miao,[3*] Zhi-Mei Sun,[3] Jia-Fu Wang,[4] Xiang-Shui Miao[1]*

[1] Wuhan National Research Center for Optoelectronics, School of Optical and Electronic Information, Huazhong University of Science and Technology, Wuhan 430074, China

[2] IMEP-LAHC, Grenoble INP – Minatec, 3 Parvis Louis Néel, 38016 Grenoble Cedex 1, France

[3] School of Materials Science and Engineering, Beihang University, Beijing 100191, China

[4] School of Science, Wuhan University of Technology, Wuhan 430070, China

*Correspondence and requests for materials should be addressed to K.-H. Xue and N.-H. Miao (email: xkh@hust.edu.cn; nhmiao@buaa.edu.cn)

Abstract

Two-dimensional materials with a proper band gap and high carrier mobility are urgently desired in the field of nanoelectronics. We propose a novel two-dimensional crystal monolayer TlP_5, which is dynamically and thermodynamically stable and possesses a direct band gap of 2.02 eV with high carrier mobilities (13960 $cm^2 V^{-1}s^{-1}$ for electrons and 7560 $cm^2 V^{-1}s^{-1}$ for holes), comparable to that of phosphorene. The band gap value and band characteristics of monolayer TlP_5 can be adjusted by biaxial and uniaxial strains, and excellent optical absorption over the visible-light range is predicted. These properties, especially for the balanced high mobilities for not only the electrons but also the holes, render monolayer TlP_5 an exciting functional material for future nanoelectronics and optoelectronic applications.

Keywords: 2D materials, thallium penta-phosphorus, monolayer TlP_5, mobility, electronic properties, phosphorene, density functional theory

This is the self-archived version of the paper

J.-H. Yuan, A. Cresti, K.-H. Xue, Y.-Q. Song, H.-L. Su, L.-H. Li, N.-H. Miao, Z.-M. Sun, J.-F. Wang, and X.-S. Miao, Journal of Materials Chemistry C 2019, 7, 639-644

DOI: 10.1039/C8TC05164J

Introduction

Since the successful mechanical exfoliation of graphene in 2004,[1,2] two-dimensional (2D) materials such as silicene,[3] borophene,[4,5] phosphorene,[6,7] and transitional metal dichalcogenides (TMDCs)[8–11] have attracted intensive interests because of their extraordinary electrical, mechanical and thermal properties that enable extensive application potential in various fields.[9,12-18] For example, phosphorene, with a direct 2.0 eV band gap as well as a high carrier mobility of about 1.14×10^3 $cm^2 V^{-1} s^{-1}$—2.60×10^4 $cm^2 V^{-1} s^{-1}$, has been considered to be a candidate for high performance field effect transistors.[6] Yet, its chemical instability under ambient conditions and the low electron mobility still hinder its practical application. MoS_2 possesses a suitable direct band gap (1.8 eV) for microelectronic and optoelectronic applications, but it suffers from the low carrier mobility (~200 $cm^2 V^{-1} s^{-1}$). Nowadays, 2D materials with a proper band gap and high carrier mobilities for both electrons and holes are still urgently desired for logic and optoelectronic devices.

Very recently, a series of 2D phosphides, such as InP_3,[19] GeP_3,[20] SnP_3,[21] and CaP_3,[22] have been theoretically proposed as novel 2D semiconductors with high carrier mobilities ($\sim10^3$ $cm^2 V^{-1} s^{-1}$—10^4 $cm^2 V^{-1} s^{-1}$) that are comparable to those of phosphorene. In addition, their theoretical cleavage energy is relatively low (0.57-1.32 J m^{-2}), indicating that they can be obtained through mechanical exfoliation from bulk. On the other hand, a layered material composed of P and Tl with the TlP_5 stoichiometry was already reported in 1971 by Olofsson *et al*.[23] Experimentally, TlP_5 single crystal can be obtained under simple and easy synthetic conditions, which facilitates its mass production. However, there has been no relevant researches published on monolayer TlP_5 yet, and it is highly worthwhile to obtain a comprehensive understanding of the monolayer form.

In this work, we report a new monolayer phosphide, namely, 2D TlP_5 with a unique structure and high dynamic and thermal stability, using first-principles calculations. In addition, TlP_5 shows remarkably weak interlayer interactions, which result in a relatively low cleavage energy of 0.39 J m^{-2}. Our calculations suggest that TlP_5 monolayer is a semiconductor with 2.02 eV direct band gap. Moreover, it possesses remarkably high carrier mobilities of 13960 $cm^2 V^{-1} s^{-1}$ and 7560 $cm^2 V^{-1} s^{-1}$ for electrons and holes, respectively. It also shows strong light absorption in the visible-light and infrared regions, which is useful for optoelectronic devices.

Results and discussion

As shown in Figures 1a-1c, the symmetry for bulk TlP_5 is orthorhombic with space group $Pmc2_1$, and the unit cell consists of four TlP_5 formula units. Our optimized lattice parameters of bulk TlP_5 are a = 6.48 Å , b= 7.01 Å and c = 12.24 Å, in good accordance with the experimental results (a = 6.46 Å , b= 6.92 Å and c = 12.12 Å).[23] In bulk TlP_5, the P atoms are connected to each

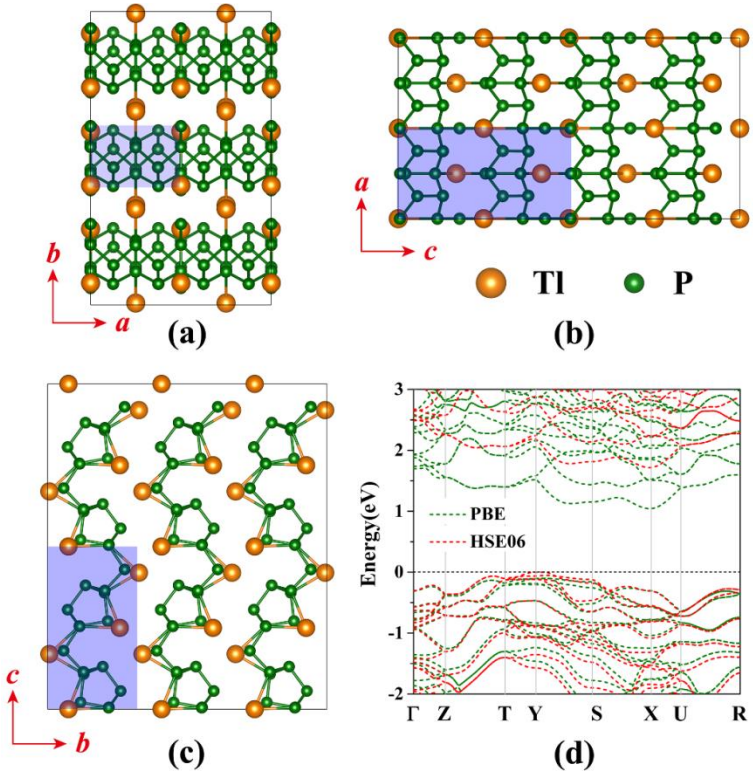

Figure 1 (a) Top and side views (along *c* and *b* directions) of optimized bulk TlP_5 with 2×3×2 supercell, respectively. The unit cell is marked in light blue squares. (d) Calculated electronic band structures of bulk TlP_5 using GGA-PBE and HSE06, respectively. The Fermi levels are set to zero energy.

other in a two dimensional network which is parallel to the (010) plane, while the two non-equivalent Tl atoms are bonded to their two neighboring P atoms in the same phosphorus layer. The phosphorus network existing in TlP_5 is very similar to that observed in the monoclinic modification of Hittorf's phosphorus[24] (see Figures S2 and S3 for details, Supporting Information). Thus, TlP_5 may be regarded as a particular 'phosphorene' whose surface has been passivated by metal thallium. The unique structural properties of TlP_5 may bring about distinct material characteristics. In addition, bulk TlP_5 is an indirect band gap semiconductor with a band gap value calculated to be 1.14 eV and 1.72 eV at the PBE and HSE06 levels (Figure 1d), respectively.

Monolayer TlP_5 was obtained in our calculation by taking an atomic layer from bulk TlP_5 along the (010) direction. As shown in Figure 2a, its structural characteristics remain, exhibiting a rectangular configuration. The optimized lattice parameters of monolayer TlP_5 are a =12.35 Å and b = 6.51 Å. The P-P bond length is 2.16 Å to 2.24 Å, shorter than that of phosphorene (2.24 Å to 2.28 Å), while the Tl-P bond length is 3.00 Å to 3.17 Å (see Table S1, Supporting Information). As is well known, mechanical cleavage[1,6] and liquid phase exfoliation [25] are powerful techniques to produce single and few layer flakes from the layered bulk materials. To assess such possibility we have calculated the cleavage energy of monolayer TlP_5 from a five-layer TlP_5 slab, mimicking the

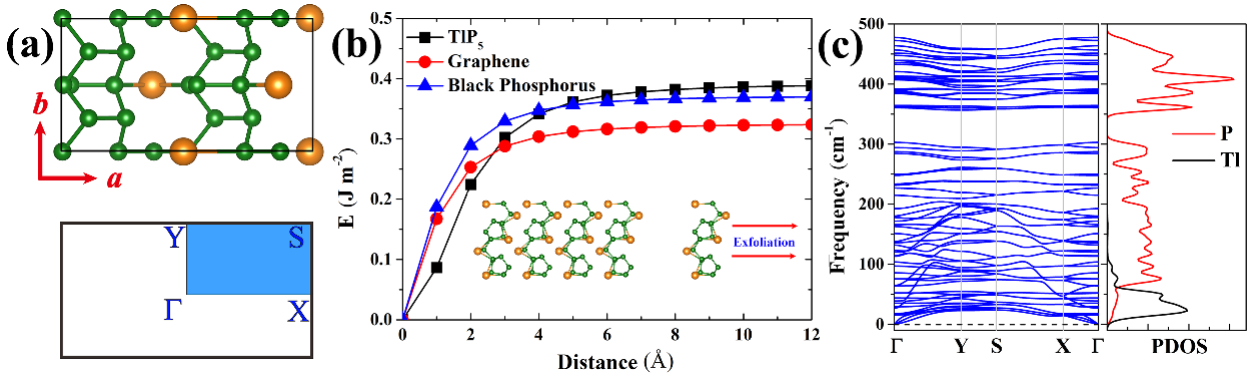

Figure 2 (a) Top view of the optimized monolayer TlP_5 and the corresponding first Brillouin zone with high symmetry points. (b) Cleavage energy estimation for the formation of monolayer TlP_5, calculated by enlarging the interlayer distance between the monolayer system that is removed from the remainder of a five-layer slab, resembling the bulk model. (c) The calculated phonon dispersion spectra and phonon density of states of the monolayer TlP_5.

bulk. As shown in Figure 2b, the cleavage energy increases with the interlayer distance, but reaching a convergence of about 0.39 J m^{-2}. The estimated exfoliation energies of graphene and black phosphorus are, respectively, 0.32 J m^{-2} and 0.37 J m^{-2} according to our calculation, which are in line with previous theoretical studies.[19,26] The DFT-estimated exfoliation energies for some other layered phosphides such as InP_3,[19] GeP_3,[20] CaP_3[22] and SnP_3[21] are 1.32 J m^{-2}, 1.14 J m^{-2}, 1.30 J m^{-2} and 0.57 J m^{-2}, respectively. Therefore, exfoliation from the bulk is feasible for monolayer TlP_5 preparation, as its cleavage energy is comparable with the mentioned 2D materials above.

In addition, the phonon dispersions of monolayer TlP_5 (shown in Figure 2c) consist of only real modes whose styles are typical for 2D crystals, indicating the kinetic stability. The highest frequency mode of monolayer TlP_5 reaches 477 cm^{-1}, which is very close to that of MoS_2 (473 cm^{-1})[27] and higher than that of phosphorene (~450 cm^{-1})[16], revealing the mechanical robustness of the covalent P-P bonds. The thermal stability is further substantiated by *ab initio* molecular dynamics (AIMD) simulations (see Figure S5, Supporting Information), where the monolayer TlP_5 structure remains intact at 300 K after a 5 *ps* simulation time.

Subsequently, we studied the electronic band structures of monolayer TlP_5. Since Tl is a heavy element, the spin-orbit coupling (SOC) effect may affect the electronic properties of monolayer TlP_5. The band structures of monolayer TlP_5 with and without SOC were both calculated, using either the PBE functional or the HSE06 hybrid functional. As shown in Figure 3a, using GGA-PBE without considering SOC, the band gap of TlP_5 is predicted to be a 1.37 eV direct one. A similar band structure but with a larger direct band gap of 2.02 eV has been confirmed based on HSE06 calculations. We then examine the effect of SOC in our calculations. The conduction band minimum (CBM) and valence band maximum (VBM) of monolayer TlP5 do not

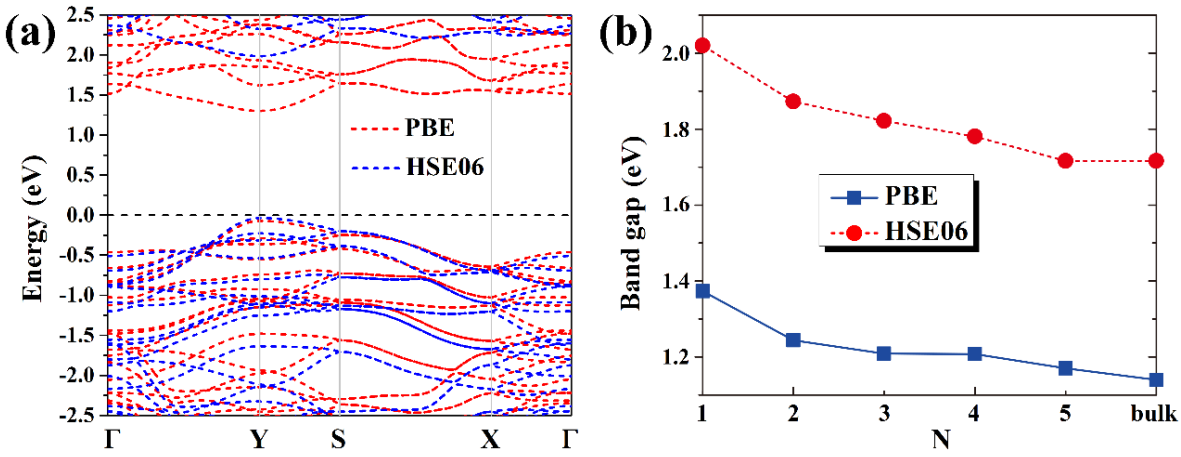

Figure 3 (a) Electronic band structures of monolayer TlP_5 calculated using GGA-PBE and HSE06 without considering SOC. (b) Computed band gaps of TlP_5 multilayers versus the number of atomic layers, using GGA-PBE and hybrid HSE06 functionals, respectively.

show discernable shift after turning on the SOC, regardless of using PBE or HSE06. For the band gap, the difference is less than 0.01 eV with and without SOC (Figures S6a and S6b, Supporting Information). The negligible impact of SOC indicate that it is the P 3*p* orbitals that contribute most to the VBM and CBM states, as can be confirmed by the wave functions and partial density of states (PDOS) results (shown in Figures S7a and S7b, Supporting Information). Therefore, we shall neglect the SOC effect in all forthcoming band structure calculations.

In order to elucidate the changes in the electronic properties of TlP_5 from the bulk to few layers, we have investigated the electronic band gaps of 2D TlP_5 with varying number of layers, where the results are shown in Figure 3b and Figure S8 (Supporting Information). The electronic structures of 2D TlP_5 multilayers indeed strongly depend on the number of layers. The bi-layer and tri-layer TlP_5 still maintain the direct band gap feature, similar to the monolayer TlP_5. However, the four-layer TlP_5 (Figure S8c, Supporting Information) shows a direct-to-indirect band gap transition with the VBM shifted from Y to A (which lies along the Y-Γ direction), though the CBM remains at the Y-point. The five-layer TlP_5 remains as an indirect band gap semiconductor (Figure S8d, Supporting Information). The possible reasons for losing the direct gap feature are the lacking of interlayer interaction, and structural reconstruction upon stacking atomic layers.[22]

In order to explore the application potential of monolayer TlP_5 in electronic devices, we systematically calculated the carrier mobility (electrons and holes) based on the deformation potential (DP) theory proposed by Bardeen and Shockley.[28] The carrier mobility of 2D materials can be evaluated by the following equation[22,29,30] $\mu_{2D} = \frac{e\hbar^3 C_{2D}}{k_B T m^* m_d (E_1^i)^2}$, where $\hbar$ is the reduced Planck constant, k_B is the Boltzmann constant, m^* is the effective mass in the direction of

Carrier type	m_a^*	m_b^*	$\|E_{1a}\|$	$\|E_{1b}\|$	C_a^{2D}	C_a^{2D}	μ_a^{2D}	μ_b^{2D}
electrons	0.480	0.645	0.574	0.614	21.59	88.49	5.24	13.69
holes	0.886	0.215	0.397	3.647	21.59	88.49	7.56	1.51

Table 1 Calculated effective mass *m** (unit: m_e), deformation potential constant $|E_l^i|$ (unit: eV), elastic modulus C_{2D} (unit: N m^{-1}), and carrier mobility μ_{2D} (unit: 10^3 cm^2 V^{-1} s^{-1}) of TlP_5 monolayer along the *a* (Y–S) and *b* (Y–Γ) directions.

transport, m_d is the average effective mass determined by $m_d=(m_a^* m_b^*)^{1/2}$, and *T* is the temperature (*T* = 300 K). The elastic modulus C_{2D} of the longitudinal strain in the propagation direction is derived from $(E-E_0)/S_0 = C_{2D}(\Delta l/l_0)^2/2$, where E is the total energy of the 2D structure, and S_0 is the lattice area of the equilibrium supercell. The deformation potential constant E_l^i is defined as $E_l^i = \Delta E_i/(\Delta l/l_0)$. Here ΔE_i is the energy change of the i^{th} band under proper cell compression and dilatation (calculated using a step of 0.25%), l_0 is the lattice constant in the transport direction and Δl is the deformation of l_0.

As summarized in Table 1, the elastic moduli are obviously anisotropic with the value of 21.59 N m^{-1} and 88.49 N m^{-1} along the *a* and *b* directions, respectively. These are slightly lower than those of phosphorene (C_x = 29 N m^{-1} and C_y = 102 N m^{-1})[29]. The effective masses of both electron and hole along the *a*/*b* directions are anisotropic as well. Especially for the hole, the effective mass along *a* direction (0.886 m_e) is notably larger than that along the *b* direction (0.215 m_e). The deformation potential E_l is nearly the same for the electron (0.574 eV along *a* and 0.614 eV along *b*), but exhibits a strong anisotropy for the hole (similar to hittorfene[24], phosphorene[29] and CaP_3[22]) with that of the *b* direction having the smallest value of about 0.397 eV. This contributes to a very large hole mobility along the *a* direction, up to 7.56×10^3 cm^2 V^{-1} s^{-1}. Note that the electron mobility along *b* direction points to an even larger value of 1.396×10^4 cm^2 V^{-1} s^{-1}, which is because of the joint action of a large elastic modulus and a small deformation potential along the *b* direction. It is also noteworthy that even the lower electron mobility in *a* direction (5.24×10^3 cm^2 V^{-1} s^{-1}) and hole mobility in *b* direction (1.51×10^3 cm^2 V^{-1} s^{-1}) are of similar order of magnitude compared with other 2D phosphides, while much larger than that of most 2D TMDCs[31].

Compared with phosphorene and their derivatives reported recently, monolayer TlP_5 possesses one of the most attractive electronic properties (see Table S3, Supporting Information). Traditionally, phosphorene and their derivatives have either high hole mobility combined with low electron mobility, or vice versa. For instance, monolayer CaP_3 has a high electron mobility of

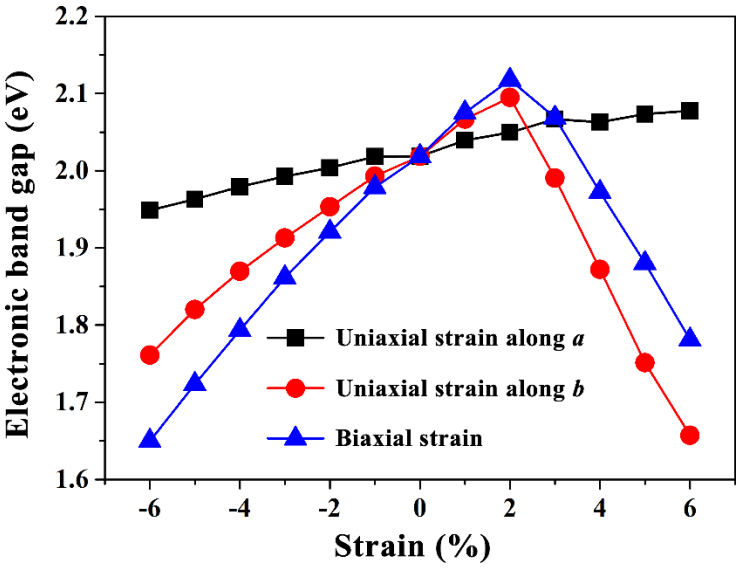

Figure 4 Electronic band gaps of monolayer TlP_5 under various strains, calculated using screened HSE06 hybrid functional.

1.99×10^4 cm^2 V^{-1} s^{-1}, whereas its hole mobility is only 0.78×10^3 cm^2 V^{-1} s^{-1}.[22] However, high hole and electron mobilities of nearly or more than the order of 10^4 cm^2 V^{-1} s^{-1} can be achieved simultaneously in monolayer TlP_5, which is of great significance for improved device performance. Furthermore, the structure of 2D TlP_5 is different from the reported 2D InP_3 or CaP_3.[19,22] There is a continuous framework of P in TlP_5, involving two different P clusters, *i.e.* P_6 and P_5. Besides, anisotropic structures also lead to anisotropic electronic structures and mechanical properties as already discussed. Note that the monolayer TlP_5 possesses a direct band gap of 2.02 eV (calculated using HSE06, where the same criteria follow below), much higher than that of InP_3 (indirect, 1.14 eV), GeP_3 (indirect, 0.55 eV), CaP_3 (direct, 1.15 eV), SnP_3 (indirect, 0.72 eV) and phosphorene (direct, 1.51 eV). Therefore, monolayer TlP_5 would be particularly suitable for nanoelectronic and optoelectronic applications.

Since applying elastic strain is an effective means of band structure engineering in 2D semiconductors,[14,32] we further studied the effects of in-plane compressive/tensile biaxial and uniaxial strains on the band structures of monolayer TlP_5. Figure 4 presents the HSE06-predicted band gaps of TlP_5 monolayer under different strains in the range of -6% to 6% (the band structures are plotted in Figure S10, Supporting Information). Interestingly, the band gaps of TlP_5 monolayer increase gradually with either compressive or tensile uniaxial strains along *a* axis, and the direct band gap feature remains unchanged within the range of strain being considered (see Figure S10a, Supporting Information). On the other hand, under the biaxial strain and the uniaxial strain along *b* axis, the band gap value demonstrates a similar variation trend, *i.e.*, increasing linearly until up to 2%, and then both decreasing linearly. A direct-to-indirect band gap transition has been discovered when the tensile strain reaches 3% for both biaxial and uniaxial strains along *b* axis. The position of the VBM is located at the Y-point while the CBM has shifted from Y to Γ (see Figures S10b and S10c, Supporting Information). The indirect band gap feature is maintained

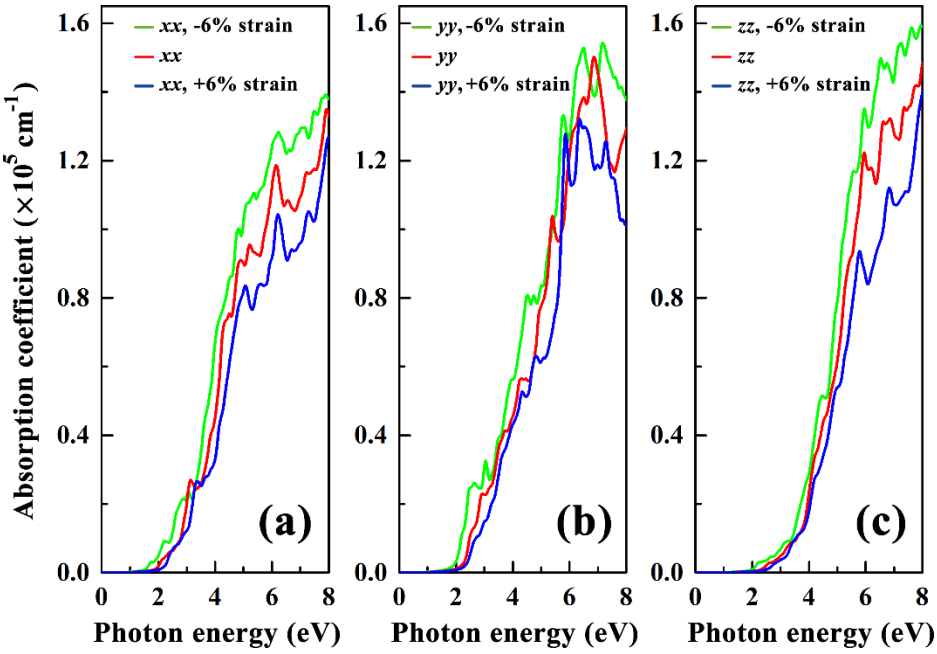

Figure 5 Calculated in-plane ((a) and (b)) and out-plane (c) light absorption coefficients of monolayer TlP_5, using the screened HSE06 hybrid functional.

with the continuous increase of strain. The variable responses to the strain in monolayer TlP_5 may be of interest for certain mechanical applications.

The direct band gap feature of monolayer TlP_5 allows it to be directly coupled to light, like phosphorene.[6] Hence, we further explored the optical properties of TlP_5 monolayer by calculating the absorption spectra in- and out-of-plane using the HSE06 functional. The transverse dielectric function $\varepsilon(\omega)=\varepsilon_1(\omega)+i\varepsilon_2(\omega)$ is used to describe the optical properties of materials,[33] where ω is the photon frequency, $\varepsilon_1(\omega)$ is the real part and $\varepsilon_2(\omega)$ is the imaginary part of the dielectric function, respectively. The absorption coefficient can be evaluated according to the expression[33] $\alpha(\omega)=\frac{\sqrt{2\omega}}{c}\left\{\left[\varepsilon_1^2(\omega)+\varepsilon_2^2(\omega)\right]^{\frac{1}{2}}-\varepsilon_1(\omega)\right\}^{\frac{1}{2}}$. As shown in Figure 5, the absorption coefficients of monolayer TlP_5 reaches the order of 10^5 cm^{-1}, and covering a wide wave-length range in the visible light region. In-plane absorption is always stronger than that of out-of-plane, due to the larger cross section area. In addition, in-plane optical absorption shows obvious anisotropy along the *x* and *y* directions, as shown in Figures 5a and 5b. Interestingly, under the applied biaxial compressive strain, both the in-plane and out-plane absorption coefficients are greatly enhanced in the all photon-energy range, which may be attributed to the band gap reduction caused by the strain (see Figure S10c, Supporting Information). However, although the band gap decreases under the biaxial tensile strain as well, a slight reduction in optical absorption has been observed, which may stem from the direct-indirect band gap transition under strain (Figure S10c, Supporting Information). The outstanding optical properties suggest potential applications of monolayer TlP_5 as efficient optical absorber materials in solar cells and optoelectronic devices.

Conclusion

In summary, we have shown that the 2D semiconducting monolayer TlP_5 is a remarkable new candidate for high performance nanoelectronics and optoelectronic devices. Synthesis of the layered bulk semiconductor species has been known since 1971, and the predicted cleavage energies indicate that exfoliation from the bulk is possible. Monolayer TlP_5 shows a direct band gap of 2.02 eV with a quite balanced and outstanding carrier mobilities for electrons (1.396×10^4 cm^2 V^{-1} s^{-1}) and holes (0.756×10^4 cm^2 V^{-1} s^{-1}), even superior to that of phosphorene. Energy gap characteristics can be modulated for the monolayer by strain engineering. Besides, TlP_5 monolayer has a substantial light absorption in the range of the solar spectrum.

Methods: All density functional theory (DFT) calculations were performed using plane-wave-based Vienna *Ab-initio* Simulation Package (VASP).[34,35] The generalized gradient approximation (GGA) within the Perdew-Burke-Ernzerhof (PBE)[36] functional form was used for the exchange-correlation energy, and projector augmented-wave (PAW) pseudopotentials[37,38] were used to replace the core electrons. The HSE06 screened hybrid functional[35] was used to calculate the band structures in order to correct the band gaps in GGA-PBE. The plane wave energy cutoff was fixed to be 500 eV. The van der Waals (vdW) interactions were corrected by the DFT-D3 approach.[39] For all structural relaxations, the convergence criterion for total energy was set to 1.0×10^{-6} eV, and structural optimization was obtained until the Hellmann-Feynman force acting on any atom was less than 0.01 eV/Å in each direction. The phonon dispersion was calculated with the density functional perturbation theory, using the PHONOPY code.[40] *Ab initio* molecular dynamics (AIMD) simulations were performed to examine the thermal stability of the structures, where NVT canonical ensembles were used.

Acknowledgement

This work was supported by the National Key Research and Development Program of China (Materials Genome Initiative, 2017YFB0701700), the National Natural Science Foundation of China under Grant No. 11704134, the Fundamental Research Funds of Wuhan City under Grant No. 2017010201010106, and the Fundamental Research Funds for the Central Universities of China under Grant No. HUST:2016YXMS212. K.-H. Xue received support from China Scholarship Council (No. 201806165012).

References

(1) Novoselov, K. S.; Geim, A. K.; Morozov, S. V.; Jiang, D.; Zhang, Y.; Dubonos, S. V.; Grigorieva, I. V.; Firsov, A. A. Electric Field Effect in Atomically Thin Carbon Films. *Science* **2004**, *306* (5696), 666-669.

(2) Novoselov, K. S.; Geim, A. K.; Morozov, S. V.; Jiang, D.; Katsnelson, M. I.; Grigorieva, I. V.; Dubonos, S. V.; Firsov, A. A. Two-Dimensional Gas of Massless Dirac Fermions in Graphene. *Nature* **2005**, *438* (7065), 197-200.

(3) Vogt, P.; De Padova, P.; Quaresima, C.; Avila, J.; Frantzeskakis, E.; Asensio, M. C.; Resta, A.; Ealet, B.; Le Lay, G. Silicene: Compelling Experimental Evidence for Graphenelike Two-Dimensional Silicon. *Physical Review Letters* **2012**, *108* (15).

(4) Mannix, A. J.; Zhou, X.-F.; Kiraly, B.; Wood, J. D.; Alducin, D.; Myers, B. D.; Liu, X.; Fisher, B. L.; Santiago, U.; Guest, J. R.; et al. Synthesis of Borophenes: Anisotropic, Two-Dimensional Boron Polymorphs. *Science* **2015**, *350* (6267), 1513-1516.

(5) Feng, B.; Zhang, J.; Zhong, Q.; Li, W.; Li, S.; Li, H.; Cheng, P.; Meng, S.; Chen, L.; Wu, K. Experimental Realization of Two-Dimensional Boron Sheets. *Nature Chemistry* **2016**, *8* (6), 563-568.

(6) Li, L.; Yu, Y.; Ye, G. J.; Ge, Q.; Ou, X.; Wu, H.; Feng, D.; Chen, X. H.; Zhang, Y. Black Phosphorus Field-Effect Transistors. *Nature Nanotechnology* **2014**, *9* (5), 372-377.

(7) Jiang, J.-W.; Park, H. S. Negative Poisson's Ratio in Single-Layer Black Phosphorus. *Nature Communications* **2014**, *5*, 4727.

(8) Manzeli, S.; Ovchinnikov, D.; Pasquier, D.; Yazyev, O. V.; Kis, A. 2D Transition Metal Dichalcogenides. *Nature Reviews Materials* **2017**, *2*, 17033.

(9) Wang, Q. H.; Kalantar-Zadeh, K.; Kis, A.; Coleman, J. N.; Strano, M. S. Electronics and Optoelectronics of Two-Dimensional Transition Metal Dichalcogenides. *Nature Nanotechnology* **2012**, *7* (11), 699-712.

(10) Radisavljevic, B.; Radenovic, A.; Brivio, J.; Giacometti, V.; Kis, A. Single-Layer MoS_2 Transistors. *Nature Nanotechnology* **2011**, *6* (3), 147-150.

(11) Schaibley, J. R.; Yu, H.; Clark, G.; Rivera, P.; Ross, J. S.; Seyler, K. L.; Yao, W.; Xu, X. Valleytronics in 2D Materials. *Nature Reviews Materials* **2016**, *1* (11), 16055.

(12) Andrew, R. C.; Mapasha, R. E.; Ukpong, A. M.; Chetty, N. Mechanical Properties of Graphene and Boronitrene. *Phys. Rev. B* **2012**, *85* (12), 125428.

(13) Huang, L.-F.; Gong, P.-L.; Zeng, Z. Phonon Properties, Thermal Expansion, and Thermomechanics of Silicene and Germanene. *Phys. Rev. B* **2015**, *91* (20), 205433.

(14) Yuan, J.; Yu, N.; Xue, K.; Miao, X. Ideal Strength and Elastic Instability in Single-Layer 8- Pmmn Borophene. *RSC Advances* **2017**, *7* (14), 8654-8660.

(15) Fei, R.; Yang, L. Strain-Engineering the Anisotropic Electrical Conductance of Few-Layer Black Phosphorus. *Nano Letters* **2014**, *14* (5), 2884-2889.

(16) Qin, G.; Yan, Q.-B.; Qin, Z.; Yue, S.-Y.; Hu, M.; Su, G. Anisotropic Intrinsic Lattice Thermal Conductivity of Phosphorene from First Principles. *Physical Chemistry Chemical Physics* **2015**, *17* (7), 4854-4858.

(17) Lopez-Sanchez, O.; Lembke, D.; Kayci, M.; Radenovic, A.; Kis, A. Ultrasensitive Photodetectors Based on Monolayer MoS2. *Nature Nanotechnology* **2013**, *8* (7), 497-501.

(18) Zhang, W.; Huang, J.-K.; Chen, C.-H.; Chang, Y.-H.; Cheng, Y.-J.; Li, L.-J. High-Gain Phototransistors Based on a CVD MoS_2 Monolayer. *Advanced Materials* **2013**, *25* (25), 3456-3461.

(19) Miao, N.; Xu, B.; Bristowe, N. C.; Zhou, J.; Sun, Z. Tunable Magnetism and Extraordinary Sunlight Absorbance in Indium Triphosphide Monolayer. *J. Am. Chem. Soc.* **2017**, *139* (32), 11125-11131.

(20) Jing, Y.; Ma, Y.; Li, Y.; Heine, T. GeP_3 : A Small Indirect Band Gap 2D Crystal with High Carrier Mobility and Strong Interlayer Quantum Confinement. *Nano Letters* **2017**, *17* (3), 1833-1838.

(21) Sun, S.; Meng, F.; Wang, H.; Wang, H.; Ni, Y. Novel Two-Dimensional Semiconductor SnP_3 : High Stability, Tunable Bandgaps and High Carrier Mobility Explored Using First-Principles Calculations. *Journal of Materials Chemistry A* **2018**, *6* (25), 11890-11897.

(22) Lu, N.; Zhuo, Z.; Guo, H.; Wu, P.; Fa, W.; Wu, X.; Zeng, X. C. CaP_3 : A New Two-Dimensional Functional Material with Desirable Band Gap and Ultrahigh Carrier Mobility. *The Journal of Physical Chemistry Letters* **2018**, *9* (7), 1728-1733.

(23) Olofsson, O.; Gullman, J.; Søtofte, I.; Beronius, P.; Engebretsen, J. E.; Ehrenberg, L. The Crystal Structure of TlP5. *Acta Chemica Scandinavica* **1971**, *25*, 1327-1337.

(24) Schusteritsch, G.; Uhrin, M.; Pickard, C. J. Single-Layered Hittorf's Phosphorus: A Wide-Bandgap High Mobility 2D Material. *Nano Letters* **2016**, *16* (5), 2975-2980.

(25) Hernandez, Y.; Nicolosi, V.; Lotya, M.; Blighe, F. M.; Sun, Z.; De, S.; McGovern, I. T.; Holland, B.; Byrne, M.; Gun'Ko, Y. K.; et al. High-Yield Production of Graphene by Liquid-Phase Exfoliation of Graphite. *Nature Nanotechnology* **2008**, *3*, 563.

(26) Guo, S.; Zhu, Z.; Hu, X.; Zhou, W.; Song, X.; Zhang, S.; Zhang, K.; Zeng, H. Ultrathin Tellurium Dioxide: Emerging Direct Bandgap Semiconductor with High-Mobility Transport Anisotropy. *Nanoscale* **2018**, *10* (18), 8397-8403.

(27) Molina-Sánchez, A.; Wirtz, L. Phonons in Single-Layer and Few-Layer MoS_2 and WS_2. *Phys. Rev. B* **2011**, *84* (15), 155413.

(28) Bardeen, J.; Shockley, W. Deformation Potentials and Mobilities in Non-Polar Crystals. *Physical Review* **1950**, *80* (1), 72-80.

(29) Qiao, J.; Kong, X.; Hu, Z.-X.; Yang, F.; Ji, W. High-Mobility Transport Anisotropy and Linear Dichroism in Few-Layer Black Phosphorus. *Nature Communications* **2014**, *5* (1).

(30) Xie, J.; Zhang, Z. Y.; Yang, D. Z.; Xue, D. S.; Si, M. S. Theoretical Prediction of Carrier Mobility in Few-Layer BC_2N. *The Journal of Physical Chemistry Letters* **2014**, *5* (23), 4073-4077.

(31) Zhang, W.; Huang, Z.; Zhang, W.; Li, Y. Two-Dimensional Semiconductors with Possible High

Room Temperature Mobility. *Nano Research* **2014**, *7* (12), 1731-1737.

(32) Yuan, J.; Yu, N.; Wang, J.; Xue, K.-H.; Miao, X. Design Lateral Heterostructure of Monolayer ZrS2 and HfS2 from First Principles Calculations. *Applied Surface Science* **2018**, *436*, 919-926.

(33) Jun-Hui, Y.; Bo, G. a. O.; Wen, W.; Jia-Fu, W.; Jun-Hui, Y.; Bo, G. a. O.; Wen, W.; Jia-Fu, W. First-Principles Calculations of the Electronic Structure and Optical Properties of Y-Cu Co-Doped ZnO, First-Principles Calculations of the Electronic Structure and Optical Properties of Y-Cu Co-Doped ZnO. *Acta Physico-Chimica Sinca* **2015**, *31* (7), 1302-1308.

(34) Kresse, G.; Furthmüller, J. Efficient Iterative Schemes for Ab Initio Total-Energy Calculations Using a Plane-Wave Basis Set. *Phys. Rev. B* **1996**, *54* (16), 11169-11186.

(35) Kresse, G.; Furthmüller, J. Efficiency of Ab-Initio Total Energy Calculations for Metals and Semiconductors Using a Plane-Wave Basis Set. *Computational Materials Science* **1996**, *6* (1), 15-50.

(36) Perdew, J. P.; Burke, K.; Ernzerhof, M. Generalized Gradient Approximation Made Simple. *Phys. Rev. Lett.* **1996**, *77* (18), 3865-3868.

(37) Blöchl, P. E. Projector Augmented-Wave Method. *Phys. Rev. B* **1994**, *50* (24), 17953-17979.

(38) Kresse, G.; Joubert, D. From Ultrasoft Pseudopotentials to the Projector Augmented-Wave Method. *Phys. Rev. B* **1999**, *59* (3), 1758-1775.

(39) Grimme, S.; Antony, J.; Ehrlich, S.; Krieg, H. A Consistent and Accurate *Ab Initio* Parametrization of Density Functional Dispersion Correction (DFT-D) for the 94 Elements H-Pu. *The Journal of Chemical Physics* **2010**, *132* (15), 154104.

(40) Togo, A.; Oba, F.; Tanaka, I. First-Principles Calculations of the Ferroelastic Transition between Rutile-Type and $CaCl_2$-Type SiO_2 at High Pressures. *Phys. Rev. B* **2008**, *78* (13), 134106.

Supporting information

First of all, we have checked the stability of bulk TlP_5 through the phonon dispersion calculation. The result in Figure S1 shows only real modes, indicating good dynamic stability.

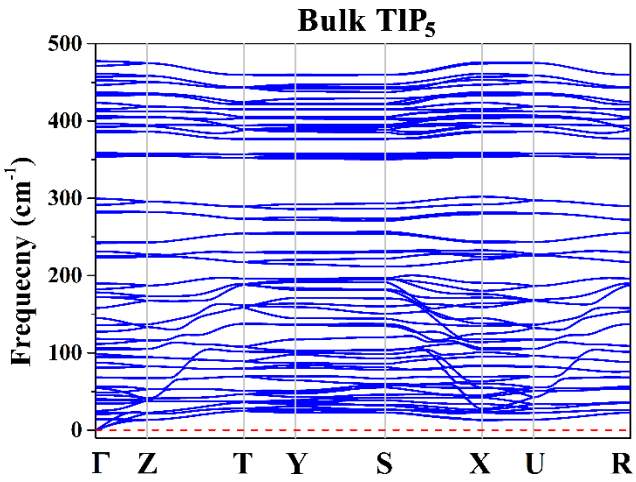

Figure S1 Calculated phonon dispersion relation of bulk TlP_5.

The phosphorus network founded in TlP_5 is very similar to the one observed in the monoclinic modification of red phosphorus, the so-called Hittorf's phosphorus.[1] As shown in Figure S2, in TlP_5 there are discernable tubes with pentagonal cross-sections, which are very characteristic structure of the phosphorus element in Hittorf's phosphorus. Comparing these two structures, one finds that the phosphorus network in TlP_5 can be regarded as stemming from a partial breaking of the network in Hittorf's phosphorus, as shown in Figure S3.

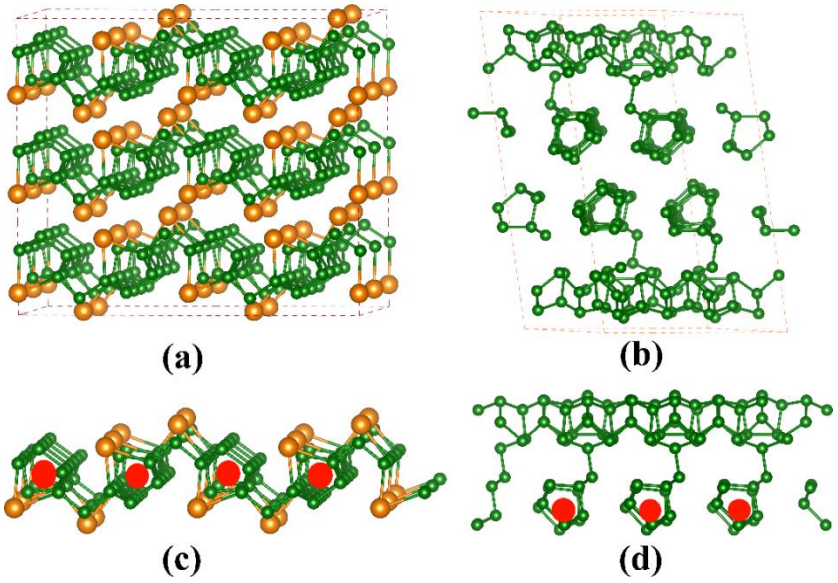

Figure S2 Demonstration of the crystal structures for: (a) bulk (2×3×2 supercell) TlP_5; (b) bulk (1×2×1 supercell) Hittorf's phosphorus; (c) monolayer (2×2×1 supercell) TlP_5; and (d) monolayer (2×2×1 supercell) Hittorf's phosphorus.

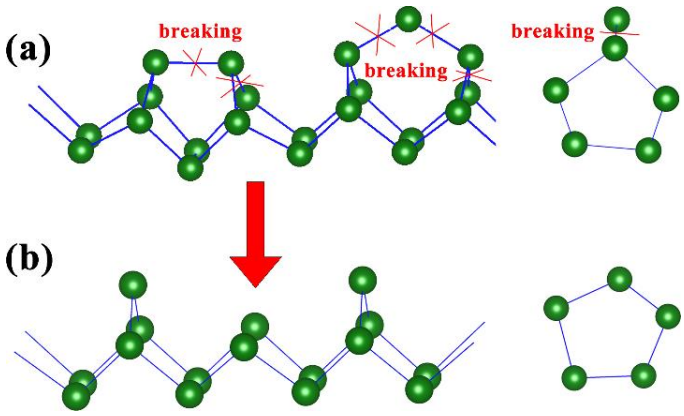

Figure S3 Comparison of the pentagonal tubes in the phosphorus network of (a) Hittorf's phosphorus and (b) TlP_5. Illustrations of the possible P-P bond breaking schemes are also given.

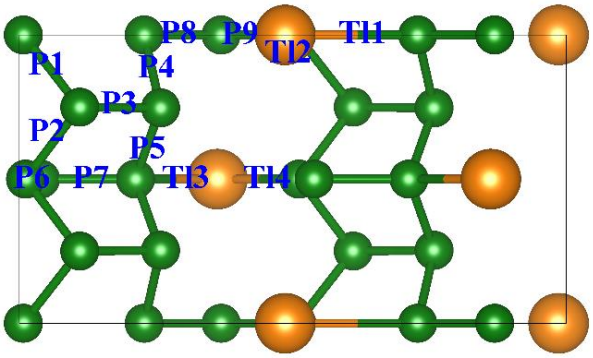

Figure S4 A schematic diagram of the P-P bonds and Tl-P bonds in monolayer and bulk TlP_5. Only a single formula unit of TlP_5 has been marked.

The bond lengths of P-P and Tl-P in both monolayer and bulk TlP_5 are listed in Table S1, together with the experimental results for the sake of comparison. The P-P bond lengths of monolayer TlP_5 are around 2.16 Å ~2.27 Å, while those of Tl-P are around 3.0 Å ~3.17 Å. These values are very close to those of optimized bulk TlP_5 (2.15 Å~2.28 Å for P-P bonds and 3.00 Å~3.09 Å for Tl-P bonds). Most of the P-P and Tl-P bond lengths in monolayer TlP_5 are slightly larger than in the bulk, which is as expected.

	1L TlP_5	Bulk TlP_5	Exp.
	P-P (Å)	P-P (Å)	P-P (Å)
P1(4)	2.243	2.242	2.242
P2(4)	2.218	2.216	2.213
P3(4)	2.27	2.275	2.229
P4(4)	2.238	2.228	2.222
P5(4)	2.227	2.218	2.225
P6(2)	2.174	2.172	2.174
P7(2)	2.157	2.15	2.126
P8(4)	2.187	2.178	2.13
P9(2)	2.203	2.198	2.221
	P-TI(Å)	P-TI(Å)	P-TI(Å)
TI1(4)	3.17	3.03	2.985
TI2(4)	3.01	3.023	3.015
TI3(2)	3.008	2.998	2.986
TI4(2)	3.04	3.089	3.025

Table S1 The optimized P-P and Tl-P bond lengths in the TlP_5 monolayer ("1L" for short) and bulk, respectively, in comparison to the experimentally verified values (Exp.) for the bulk. The numbers in parentheses count the equivalent P-P bonds in a unit cell, and the corresponding bond locations are marked in Figure S4.

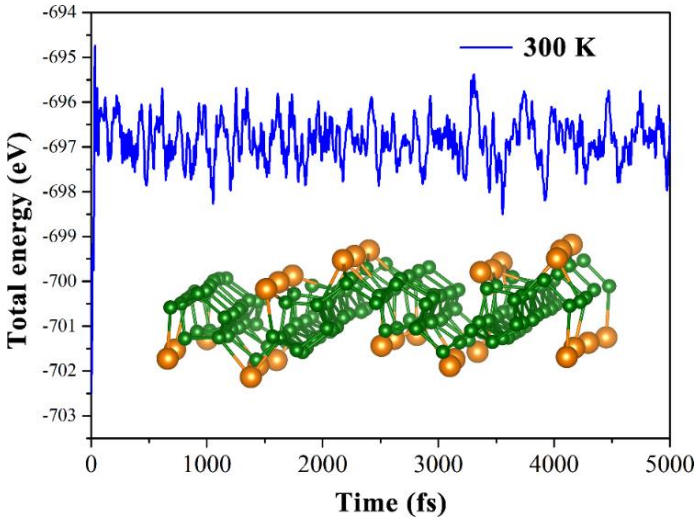

Figure S5 Side view of the snapshots from the molecules dynamics simulation for the TlP_5 monolayer. The variation of total energy was recorded during the simulation time of 5 ps, and the temperature was 300 K.

The optimized lattice constants of *n*L (*n*=1, 2, 3, 4, 5) TlP_5 and bulk are listed in Table S2, with reference to experimental values. The optimized lattice parameters of monolayer TlP_5 are *a* = 12.35 Å and *b* = 6.51 Å (note that the *a*/*b* here actually correspond to the *c*/*a* directions in bulk). Upon the increase in the number of layers, the lattice constants vary very little, indicating a relatively weak interlayer coupling in the TlP_5 system.

Lattice constant	1L	2L	3L	4L	5L	Bulk	Exp.[2]
a/Å	12.35	12.27	12.26	12.26	12.25	6.48	6.46
b/Å	6.51	6.49	6.49	6.48	6.48	7.01	6.92
c/Å	--	--	--	--	--	12.24	12.12

Table S2 The optimized lattice constants (*a*/*b*/*c*) in TlP_5 monolayer (1L), bilayer (2L), tri-layer (3L), four-layer (4L), five-layer (5L) and bulk, respectively, in comparison to the experimental values (Exp.) for the bulk.

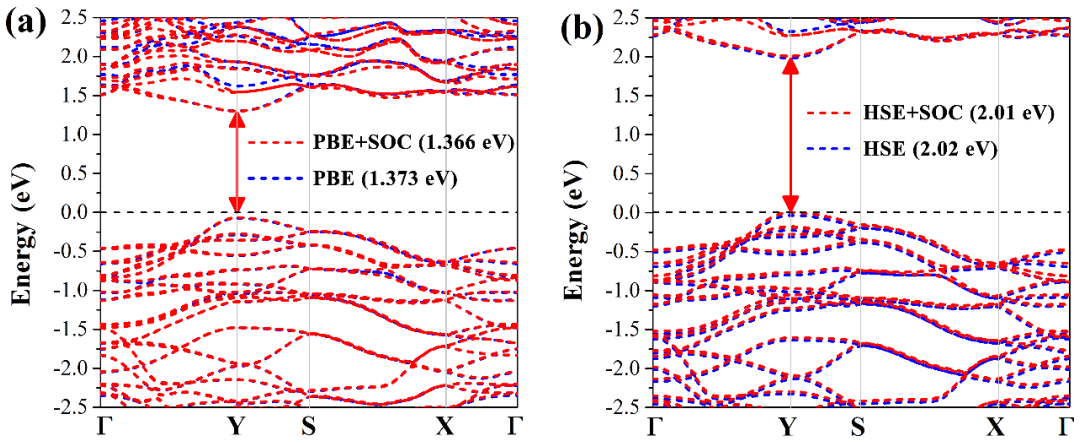

Figure S6 (a) Band structures of monolayer TlP_5 calculated using the PBE functional, either with or without considering the effect of spin orbit coupling (SOC). (b) Band structures of monolayer TlP_5 calculated using the screened HSE06 hybrid functional, either with or without considering the effect of SOC.

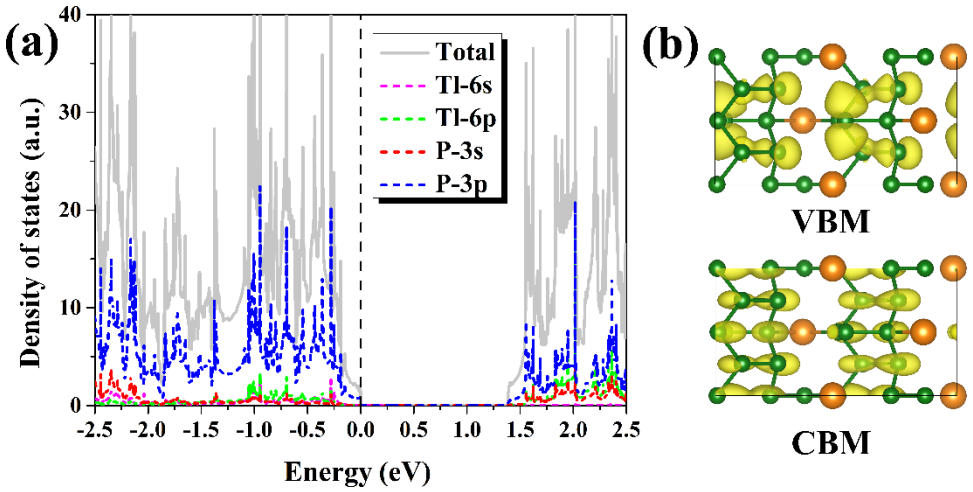

Figure S7 (a) Projected density of states of monolayer TlP_5. (b) Isosurfaces of partial charge densities corresponding to the VBM and CBM of monolayer TlP_5.

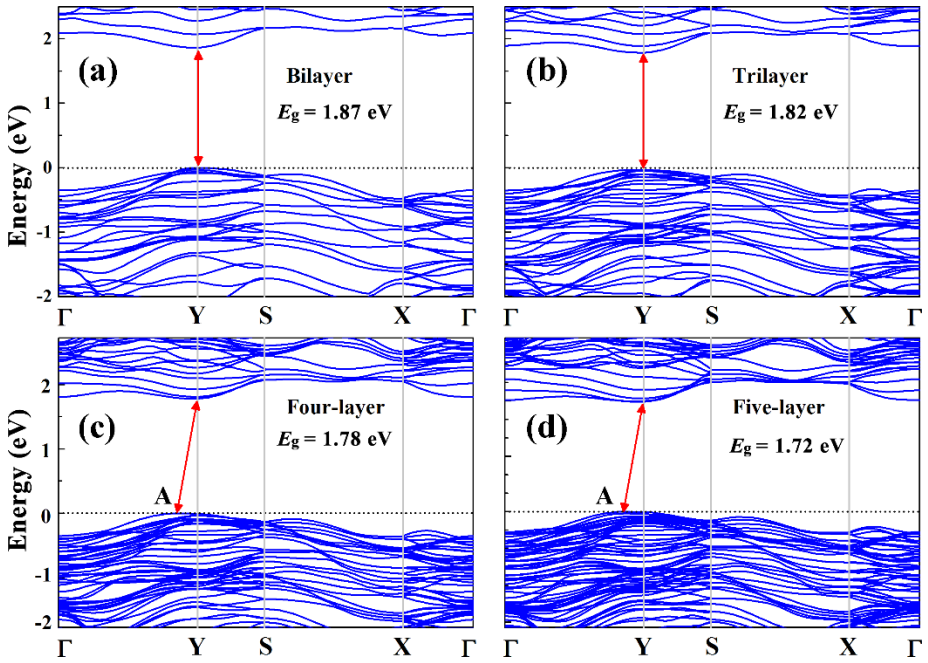

Figure S8 Electronic band structures of 2D TlP_5 with varying number of layers, calculated using the screened HSE06 hybrid functional: (a) bilayer; (b) trilayer; (c) four-layer; and (d) five-layer.

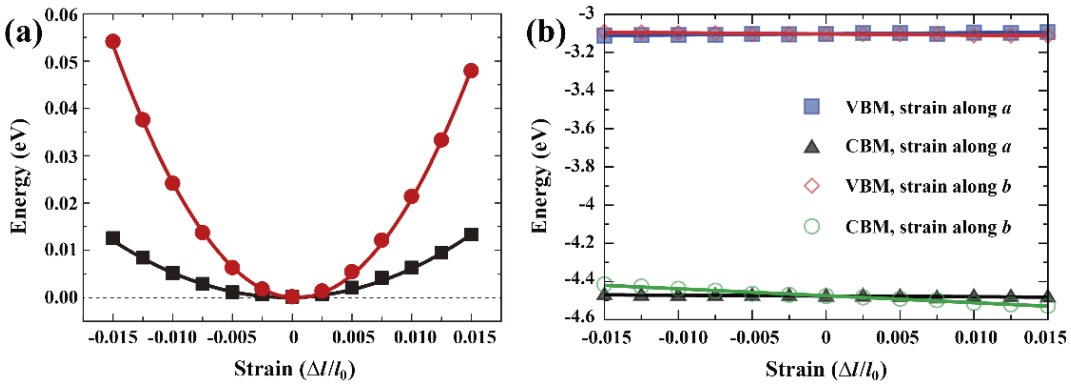

Figure S9 (a) The relationship between total energy and the applied strain δ along the *a* and *b* directions of monolayer TlP_5. The quadratic data fitting gives the in-plane stiffness of 2D structures. Black and red curves show the in-plane stiffness along the *a* and *b* directions of monolayer TlP_5, respectively. (b) The shift of VBMs and CBMs for monolayer TlP_5 with respect to the vacuum energy, as a function of the applied strain along either the *a* or the *b* direction. The linear fit of the data yields the deformation potential constant.

	Direction	TlP_5	Phosphorene[3]	Hittorfene[1]	InP_3[4]	GeP_3[5]	CaP_3[6]	SnP_3[7]
Electron	*x*	5.24	1.10-1.14	0.50	0.54	0.04	19.9	0.19
	y	13.96	0.08	0.43	1.92	0.07	1.75	0.21
Hole	*x*	7.56	0.64-0.70	0.31	0.006	0.014(0.35)	0.08	0.17
	y	1.51	10-26	7.68	0.05	0.19(2.36)	0.78	0.36
Band gap		2.02(*d*)	1.51(*d*)	2.5(*d*)	1.14(*i*)	0.55(*i*)	1.15(*d*)	0.72(*i*)

Table S3 The carrier mobilities μ_{2D} ($\times 10^3$ cm^2 $V^{-1}s^{-1}$) and energy bang gaps (eV, calculated at the HSE06 level) of phosphorene and their derivatives for comparison (only the monolayer is considered). The symbols *d* and *i* represent direct and indirect band gaps, respectively.

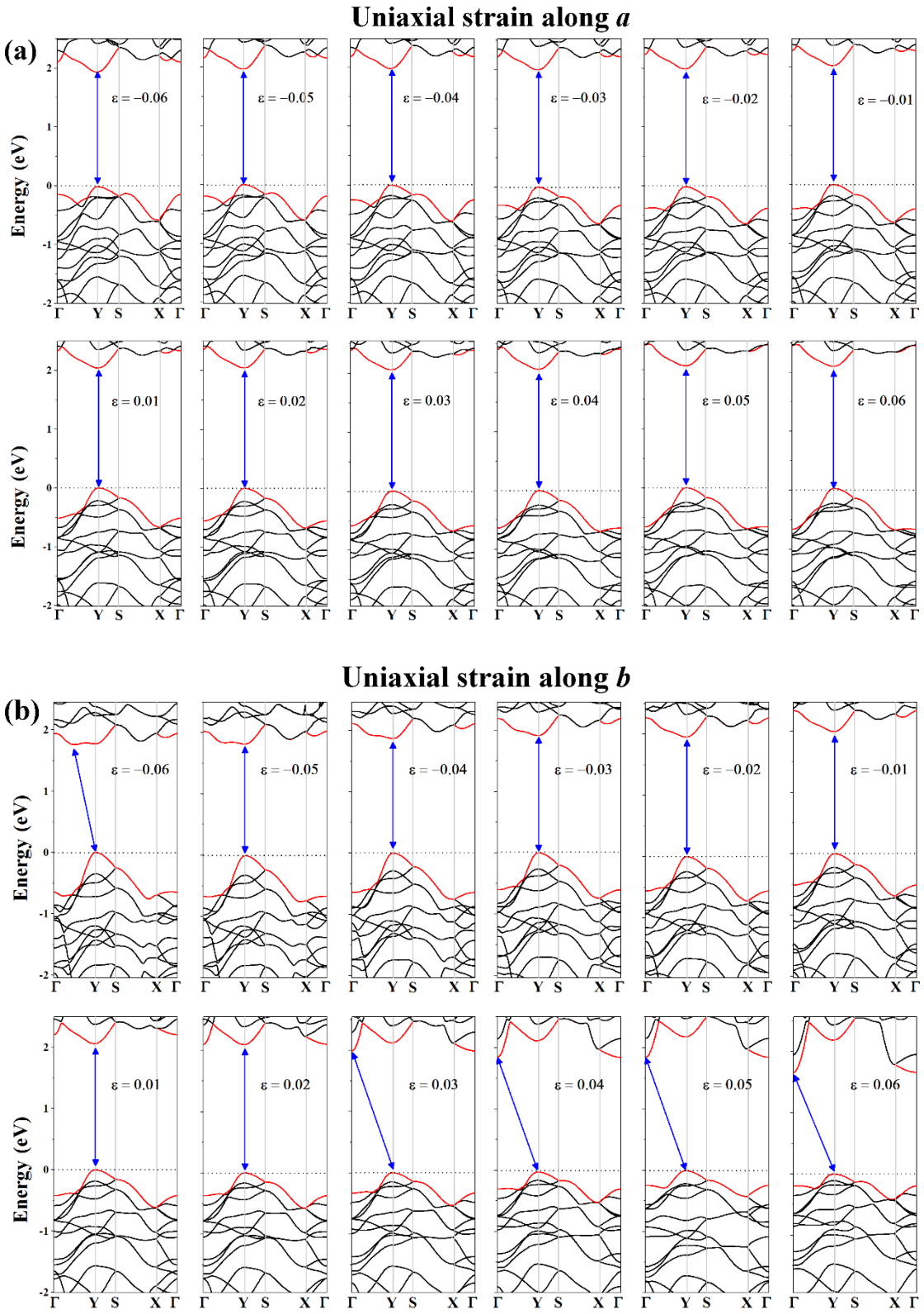
Uniaxial strain along *a*
(a)
Energy (eV)
ε = −0.06
ε = −0.05
ε = −0.04
ε = −0.03
ε = −0.02
ε = −0.01
ε = 0.01
ε = 0.02
ε = 0.03
ε = 0.04
ε = 0.05
ε = 0.06
Γ Y S X Γ
Uniaxial strain along *b*
(b)
Energy (eV)
ε = −0.06
ε = −0.05
ε = −0.04
ε = −0.03
ε = −0.02
ε = −0.01
ε = 0.01
ε = 0.02
ε = 0.03
ε = 0.04
ε = 0.05
ε = 0.06
Γ Y S X Γ

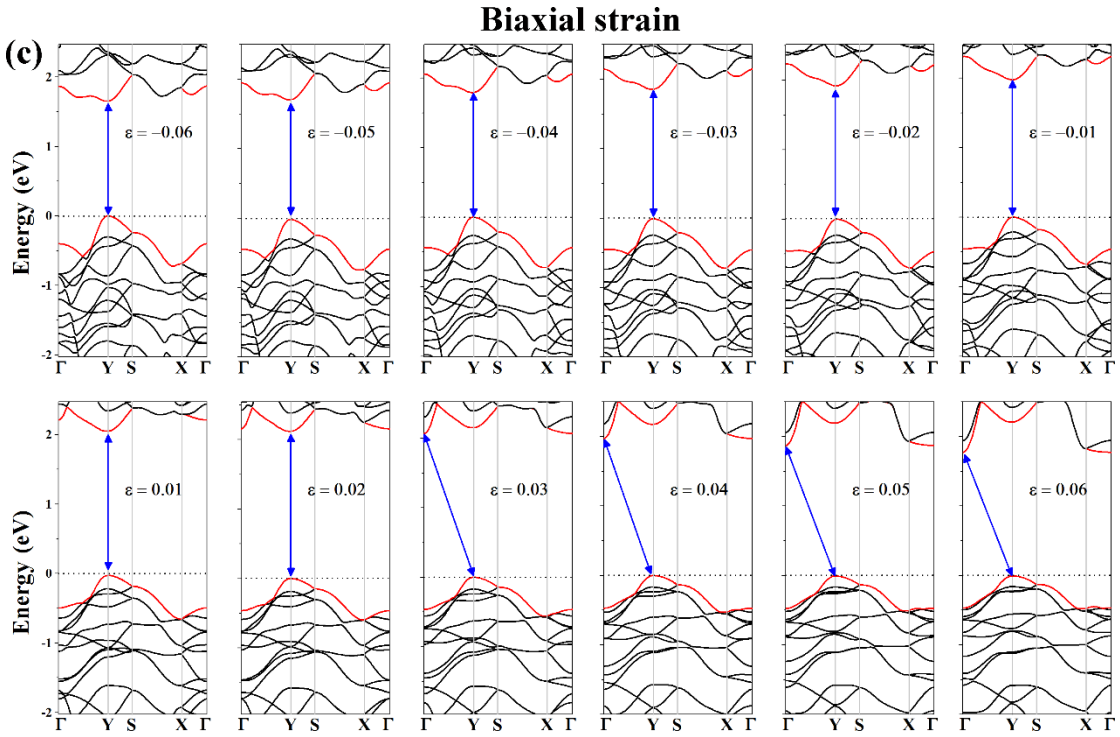

Figure S10 Electronic band structures of monolayer TlP_5 under various strain situations, calculated using the HSE06 functional. The applied strains are (a) uniaxial strain along *a*-axis; (b) uniaxial strain along *b*-axis (b); and (c) biaxial along both *a* and *b*.

References

(1) Schusteritsch, G.; Uhrin, M.; Pickard, C. J. Single-Layered Hittorf's Phosphorus: A Wide-Bandgap High Mobility 2D Material. *Nano Letters* **2016**, *16* (5), 2975-2980.

(2) Olofsson, O.; Gullman, J.; Søtofte, I.; Beronius, P.; Engebretsen, J. E.; Ehrenberg, L. The Crystal Structure of TlP5. *Acta Chemica Scandinavica* **1971**, *25*, 1327-1337.

(3) Qiao, J.; Kong, X.; Hu, Z.-X.; Yang, F.; Ji, W. High-Mobility Transport Anisotropy and Linear Dichroism in Few-Layer Black Phosphorus. *Nature Communications* **2014**, *5* (1).

(4) Miao, N.; Xu, B.; Bristowe, N. C.; Zhou, J.; Sun, Z. Tunable Magnetism and Extraordinary Sunlight Absorbance in Indium Triphosphide Monolayer. *J. Am. Chem. Soc.* **2017**, *139* (32), 11125-11131.

(5) Jing, Y.; Ma, Y.; Li, Y.; Heine, T. GeP_3 : A Small Indirect Band Gap 2D Crystal with High Carrier Mobility and Strong Interlayer Quantum Confinement. *Nano Letters* **2017**, *17* (3), 1833-1838.

(6) Lu, N.; Zhuo, Z.; Guo, H.; Wu, P.; Fa, W.; Wu, X.; Zeng, X. C. CaP_3: A New Two-Dimensional Functional Material with Desirable Band Gap and Ultrahigh Carrier Mobility. *The Journal of Physical Chemistry Letters* **2018**, *9* (7), 1728-1733.

(7) Sun, S.; Meng, F.; Wang, H.; Wang, H.; Ni, Y. Novel Two-Dimensional Semiconductor SnP_3: High Stability, Tunable Bandgaps and High Carrier Mobility Explored Using First-Principles Calculations. *Journal of Materials Chemistry A* **2018**, *6* (25), 11890-11897.